Actual Problems of Mathematical Modeling and Information Technologies (APMMIT-2025)

Illumination-Aware Channel Optimization Using Genetic Algorithms for Skin Lesion Segmentation

AIPCP25-CF-APMMIT2025-00124 | Article

PDF auto-generated using **ReView**
from
RIVER VALLEY
TECHNOLOGIES

Illumination-Aware Channel Optimization Using Genetic Algorithms for Skin Lesion Segmentation

Jasurbek Nazarov[1, a)], Shukrullo Kakharov[2 b)], Azizjon Meliboev[1, c)], Dostonbek Islomov[3, d)]

[1]*Kokand university, Kokand , Uzbekistan,*
[2]*Oriental University, Tashkent, Uzbekistan,*
[3]*Cyber university, Tashkent, Uzbekistan*

[a)] *Corresponding author: jinazarov@kokanduni.uz*
[b)] *sh.kaxarov@airi.uz*
[c)] *a.meliboyev@kokanduni.uz*
[d)] *islomovdostonbek97@gmail.com*

Abstract. Skin cancer is still the most common type of cancer in the world, and treatment results are significantly improved by early detection. Despite the impressive accuracy attained by deep learning-based segmentation algorithms, performance is still constrained by enduring issues like differences in lesion size, shape, color distribution, lighting, and contrast. This work suggests a Genetic Algorithm (GA)-based illumination-aware channel optimization framework for improved skin lesion segmentation. To increase adaptability to different input dimensions, a modified Transformer–U-Net hybrid architecture is presented, in which a specially designed feature extraction block takes the role of the traditional ResNet backbone. The architecture uses a dual-branch design, incorporating convolutional layers to extract fine-grained local features and transformer modules to capture global contextual relationships. A GA-driven channel selection technique is included to improve segmentation performance even more. In order to effectively pick between several illumination-sensitive and illumination-invariant representations, the algorithm iteratively looks for the best combination of image channels represented as binary chromosomes. The framework incorporates grayscale images, shading-attenuated images, and unique spectral band representations based on skin imaging principles in addition to normal RGB inputs. According to experimental data, segmentation performance is better when R_n, GRAY, SA, and RGB channels are combined than when RGB images are used alone. The suggested approach produced competitive and trustworthy segmentation results when tested on the openly accessible ISIC 2017 dataset.

INTRODUCTION

Protecting us from the environment, sensing stimuli, regulating body temperature through sweat, and signaling hair growth in response to cold are just a few of the vital functions of the skin, the biggest organ in our body. However, if the condition causes the skin's cells to shift irregularly and begin to grow out of control, they may turn into skin cancer, which occasionally spreads to other parts of the body. Skin cancer is a serious and pervasive threat that affects many people annually in the United States [1, 2] and around the world. In general, there are two main types of skin cancer: non-melanoma skin cancers, which originate from cells in the epidermis, and melanoma skin cancers, which are caused by malfunctioning melanocytes [3]. According to estimates, melanoma, a kind of skin cancer that accounts for a comparatively tiny percentage of all skin cancer cases in the United States, will kill 7,990 people in 2023 [4]. Compared to the 7,180 recorded deaths in the USA alone in 2021, this is an increase [5]. The importance of early diagnosis in raising patient survival rates is highlighted by research. Skin tumors can be detected visually, however it can be difficult to tell malignant lesions from healthy skin. As a result, automated dermoscopic picture interpretation has become commonplace through the extensive use of computer-aided diagnostic tools. As a result, segmenting these photos of skin lesions is crucial to the diagnosis and therapeutic procedures. To differentiate lesions from healthy skin, segmentation entails drawing pixel-by-pixel labels along the margins of the lesions. However, the many characteristics

of skin lesions, such as their color, presentation, shape, and contrast, which are controlled by a variety of circumstances, including variations within and across classes and image capture settings, make this work difficult.

While a number of traditional segmentation techniques have been used to segment medical images, including active contour [5, 6], edge-based segmentation [8, 9], thresholding [10-12, 13], optimization algorithms [14, 15, 16], and watershed segmentation [17, 18], methods using deep learning have advanced considerably and are currently the most widely used method for analyzing medical images. A fully convolutional network (FCN) is a no-table breakthrough that produced impressive results. It was first put forth in [19]. Many image segmentation models from FCN have now been proposed. FCN is notable for its distinctive feature of being fully convolutional across all layers, which does away with the requirement for a certain input image size. Despite these benefits, there are several disadvantages to the segmentation results generated by FCN.

A restricted sensitivity to complex characteristics within the image is shown by the results' tendency to lack fine details and look comparatively smooth and fuzzy. Ronneberger and associates [20] expanded on this idea by creating a U-shaped architecture for FCNs. There are symmetrical contracting and growing paths in this network topology. The contracting path produces many feature maps and reduces the dimensionality of the data. On the other hand, the expanding route makes use of a hierarchical collection of up-sampling layers in order to generate segmentation maps and capture semantic features.Numerous medical fields have made extensive use of the U-Net framework, which has produced noteworthy results [9, 21-28].

Kumar et al. [29] proposed a novel deep learning-based segmentation method in recent years. By utilizing the lighting invariance of various tissues, the model seeks to improve accuracy in the segmentation of skin lesions. In particular, nine-channel pictures derived from RGB dermoscopic images with varying illuminations were used to train the models. A. Wan et al. [30] proposed gathering contextual information about nuclei and capturing nuclei features at different scales. Despite improving segmentation accuracy, the incorporation of these high-level and high-dimensional characteristics typically results in high model complexity or necessitates spatial sampling operations to encode the spatial elements of an image into a space with low dimensions. Information loss may result from changes made to certain low-frequency components during the decoding phase. Additionally, because convolutional processes have a limited receptive field, approaches based on CNNs have difficulty establishing extensive dependencies over long distances and global context connections [31, 32-34].

A Genetic Algorithm (GA)-guided lighting selection method for skin lesion segmentation is proposed in this work. In particular, the RGB images were initially recovered from RGB dermoscopic images, and five distinct illuminations—R_n (1 channel), V_c (1 channel), intrinsic images (1 channel), grayscale images (1 channel), and Shadding-attenuated images (3 channels)—were first extracted. The six distinct illuminations are therefore regarded as distinct features to be employed in training the corresponding segmentation model, and the skin lesion segmentation procedure is formulated as a feature selection issue. The feature choice problem is revised as an optimization issue in this work, with the goal being to choose features or combinations of illumination that optimize the segmentation result's efficiency. The Genetic technique (GA), a binary-coded GA technique that has been extensively used for feature selection in the literature, is used to solve the resulting feature selection problem. Regarding the segmentation model, we use TMU-Net, a cutting-edge transformer-based U-Net model, and alter its design to support images with more than three channels. The suggested approach can evolve effective feature combinations to increase the segmentation accuracy, according to the experimental findings based on the widely utilized Inter-national Skin Imaging Collaboration (ISIC) 2017 skin segmentation dataset.

The following is an outline of the remaining portions of the paper: All of the various color bands or image channels taken into consideration in this work are shown in Section 2. Information on the GA-based feature selection is provided in Section 3. In particular, the challenge objectives and a summary of genetic algorithms are provided. The segmentation network that underlies it is also described in detail. Section 4 presents and discusses experimental findings derived from the ISIC 2017 dataset. Conclusions and next projects are discussed in Section 5.

DERMOSCOPIC IMAGE TRANSFORMATIONS

The various transformations used in this study are described in detail in the following section. A segmentation model is trained using several illuminations or transformations that are extracted from RGB dermoscopic images in addition to the original image, as was previously indicated. Our method specifically uses changes of particular color bands, an intrinsic grayscale image that is illumination-invariant, a color theory-based grayscale estimate, and a shading-attenuated image that is obtained from the dermoscopic image. We go into further detail about the methods used to create these unique photos in the ensuing subsections.

Initially, the Normalized Red channel (R_n) and the complement of the HSV Value channel (V_c) were identified as two discriminative color-band representations [31]. While the supplemented Value channel highlights darker lesion patches in HSV space, the normalized red channel highlights lesion pigmentation by scaling the red component in relation to overall intensity. The contrast between surrounding tissue and the lesion is heightened by these changes.

Red Channel Normalized

$$R_n = \frac{R}{R+G+B} \tag{1}$$

HSV Value Channel (V_c) complement:

$$V_c = 1 - V \tag{2}$$

where V is the HSV color space's value component. The contrast between the lesion and the skin that surrounds it is improved by these changes.

Second, entropy minimization, as suggested by Finlayson et al. [35], was used to create an illumination-invariant intrinsic image. By projecting log-chromaticity values onto a plane orthogonal to the illumination direction, this method distinguishes between illumination effects and reflectance. The resulting intrinsic grayscale image offers robust structural information for segmentation and is essentially unaffected by changes in lighting.

Third, using the preprocessing framework suggested by Madooei et al. [36], a reflectance-based grayscale (GRAY) representation was constructed. This method makes use of skin spectral reflectance modeling [30, 31], in contrast to traditional grayscale conversion techniques [39]. Principal Component Analysis (PCA) is used after mapping the image into optical density space. The grayscale representation is the first principal component, which accounts for most of the variance related to skin reflectance characteristics. This suppresses areas of healthy skin while increasing the visibility of lesions.

Lastly, the method outlined in [6] was used to create shading-attenuated (SA) photographs in order to reduce the impacts of uneven illumination. The RGB image is converted to HSV space, the Value channel is normalized, the histogram is aligned with the intrinsic image, and the image is then reconstructed in RGB space. This procedure enhances lesion boundary uniformity and lessens shading artifacts.

GENETIC ALGORITHM-GUIDED FEATURE SELECTION

Modified TMU-Net Architecture

By combining the complimentary advantages of transformer-based topologies and convolutional neural networks (CNNs), the Contextual Attention Network: Transformer Meets U-Net (TMU-Net), first presented in [31], marks a substantial breakthrough in medical image segmentation. In contrast to previous hybrid methods [40, 41], which had trouble successfully combining local and global contextual representations, TMU-Net uses a structured dual-branch architecture to overcome this drawback. One branch of this system uses transformer modules to acquire global contextual information using self-attention mechanisms and represent long-range spatial interdependence. Convolutional layers are used in the parallel branch to extract fine-grained local characteristics, which are essential for accurate boundary delineation. In dermoscopic pictures, this dual-pipeline arrangement enhances attention to prominent lesion locations and permits adaptive feature scaling [31].

Notwithstanding its benefits, the original TMU-Net architecture is limited to three-channel RGB inputs due to its pre-trained ResNet50 backbone. When adding more illumination-derived representations, this restriction presents difficulties. We use a specially created convolutional block in place of the pre-trained ResNet block to get around this restriction (see Fig. 1). The updated block offers flexibility in handling varied input dimensions, enabling multi-channel inputs beyond typical RGB, even though it is architecturally inspired by residual learning concepts. This change eliminates the need for fixed channel size, but it also makes training more difficult, requiring a bigger dataset and more training time to reach similar performance levels. An overview of the suggested Modified TMU-Net design is shown in Figure 1.

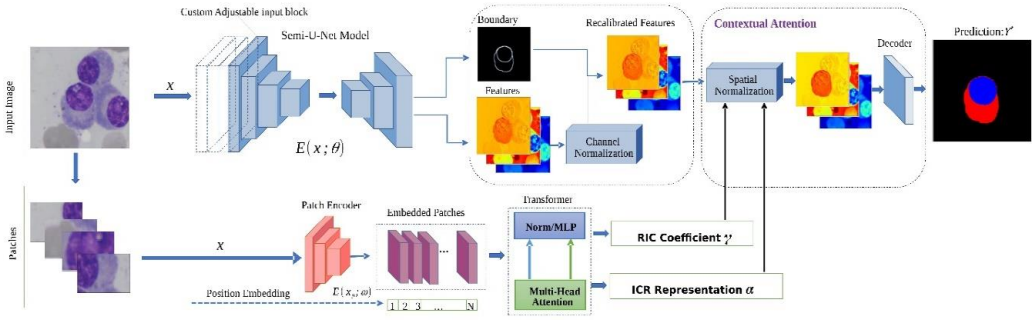


FIGURE 1. An overview of the suggested modified TMU-Net is shown in Figure 1.

Genetic Algorithm for Channel Optimization

Natural evolution and selection serve as the inspiration for the Genetic Algorithm (GA), a population-based metaheuristic optimization technique. GA iteratively evolves candidate solutions toward optimality using selection, recombination, and mutation procedures. It was first formalized for optimization and search issues. There are four main steps in the GA process used in this work:

Step 1: Initialization. A P of size N is created at random for the initial population. Every individual (chromosome) is a binary vector that encodes a potential solution. Random initialization guarantees wide search space exploration and encourages variation.

Step 2: Selection. A pre-established fitness function is used to assess each chromosome. Tournament selection, which probabilistically favors higher-performing individuals while preserving population variety, is used to choose parent solutions based on fitness ratings.

Step 3: Recombination, or crossover. Two-point crossover is performed on chosen parents, with the chance that $prob_{cross} = 1$. Offspring that blend features from both parents are produced by the exchange of genetic material at two randomly chosen locations in the chromosome. Exploration of novel channel combinations is improved by this operation.

Step 4: Mutation. Through a bit-flip operator with probability $prob_{mut} = 0.9$, mutation adds stochastic variation. The algorithm can avoid local optima and avoid premature convergence.

Algorithm 1 provides a summary of the entire GA process.

Algorithm 1 GA Algorithm
Require: N, G, $prob_{mut}$, $prob_{cross}$
Initialize population of *P* of *N* random chromosomes
$t \leftarrow 1$
$cost \leftarrow fitness(P)$
while $t \leq G$ **do**
  $p1, p2 \leftarrow selection(P, cost)$
  $offsprings \leftarrow crossover(p1, p2, prob_{cross})$
  $P_{new} \leftarrow mutation(offsrings, prob_{mut})$
  $P \leftarrow P_{new}$
  $t \leftarrow t + 1$
end while

Formulation of the Problem

This paper formulates the problem of channel selection as a combinatorial optimization problem. A binary vector of length six is used to represent each potential solution:

$x=[b_1, b_2, b_3, b_4, b_5, b_6]$

Where each binary element $b_i \in \{0,1\}$ indicates the inclusion or exclusion of a particular picture representation in the following order:

1. R_n
2. V_c
3. *Gray*
4. *Intrinsic*
5. *Shading-Attenuated (SA)*
6. *RGB*

For instance: [1,0,0,1,1,0] denotes the deployment of R_n, *SA*, and intrinsic channels. By training the modified TMU-Net with the chosen channels and calculating performance metrics on the validation set, the fitness of each solution is assessed. The definition of the cost function is:

$$F(x) = -(Acc(\theta_x) + F1(\theta_x) + Sens(\theta_x) + Spec(\theta_x)) \quad (3)$$

where:

- The trained segmentation network employing the channels given by solution x is represented by θ_x.
- Acc indicates precision,
- F1 stands for F1-score.
- Sensitivity is indicated by Sens.
- Specificity is indicated by Spec.

The negative sign guarantees minimization of the cost function, which corresponds to optimizing segmentation performance.

Overall Framework

The full framework for GA-guided channel optimization incorporates:

1. Extraction of visual representations resulting from illumination
2. Channel combinations are encoded in binary.
3. Optimization with GA
4. Modified TMU-Net training
5. Performance-based assessment of fitness

The best illumination combinations for improved skin lesion segmentation may be automatically found thanks to this iterative procedure. Figure 2 shows a summary of the suggested framework for GA-guided image channel selection.

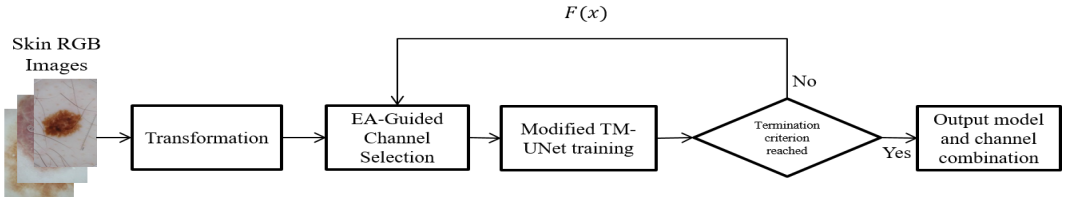


FIGURE 2. A summary of the suggested GA Guided Image Channel Selection for Skin Lesion Segmentation is shown in the Figure.

EXPERIMENTAL SETUP AND RESULTS

The performance analysis, evaluation metrics, and setup for experiments of the suggested GA-guided illumination-aware segmentation framework are covered in this part. The ISIC ISBI 2017 Challenge dataset [42], which was first made available as a component of the International Skin Imaging Collaboration (ISIC) 2017 Kaggle competition, was used for the experiments. Lesion segmentation, illness classification, and dermoscopic feature identification were the three main tasks in the challenge. We only address the lesion segmentation problem in this paper. The dataset includes 2,000 dermoscopic pictures that were obtained by methods that improve the viewing of subsurface objects by lowering surface skin reflection. In accordance with standard procedure in the literature [3], the dataset was separated into:

• Training set: 1,250 images
• Validation set: 150 images
• Test set: 600 images

All photos were scaled to 256 × 256 pixels from their original resolution of 576 × 767 pixels due to technical limitations. Preprocessing procedures were used in accordance with earlier segmentation research [28]. PyTorch was used for the implementation, and an NVIDIA RTX 4090 GPU was used for all experiments. The Adam optimizer was used to train the network with:

• Learning rate: 1×10^{-4}
• Batch size: 4
• Number of epochs: 5

Evaluation Metrics

Four commonly used metrics were used to objectively assess segmentation performance: F1-score, Accuracy, Sensitivity, and Specificity. These measurements offer a thorough evaluation of background discrimination performance as well as lesion detection capability.

An accuracy is the ratio of correctly classified attacks to the total number of instances, as indicated by the equation (4).

$$Accuracy = \frac{TP + TN}{TP + TN + FP + FN} \tag{4}$$

Similar to the Recall, it displays the proportion of properly identified attacks compared to all attacks, as shown in Equation (5).

$$Recall = \frac{TP}{TP + FN} \tag{5}$$

According to Equation (6), a precision metric equal to the number of correctly detected assaults is divided by the sum of correctly and mistakenly identified attacks.

$$Precision = \frac{TP}{TP + FP} \tag{6}$$

An evaluation metric that evaluates a model's overall performance on a particular dataset is called an F1-score. As in Eqn. (7), it takes the harmonic mean of the model's Precision and Recall and combines them into a single metric.

$$F1score = \frac{TP}{TP + \frac{1}{2}(FP + FN)} \tag{7}$$

Where:
True Positive (TP)that are accurately diagnosed as lesions,
True Negative (TN): Pixels that are appropriately categorized as backdrop,
False Positive (FP): Background pixels that were incorrectly identified as lesions,
False Negative (FN): Pixels with lesions incorrectly identified as background.

Quantitative Results and Analysis

Together with the baseline RGB-only setup, Table 1 displays the quantitative results of the 600-image test set utilizing various illumination channel combinations chosen by the Genetic Algorithm.

TABLE 1. Quantitative Results on ISIC 2017 Test Set.

Channel Combination	F1	Accuracy	Specificity	Sensitivity	Total
R_n_V_c	0.7549	0.9041	0.9459	0.7368	3.3418
V_c_GRAY_Intrinsic_SA	0.8183	0.9338	0.9808	0.7460	3.4791
R_n_GRAY_Intrinsic_SA	0.8182	0.9325	0.9760	0.7587	3.4855
R_n_GRAY	0.8154	0.9288	0.9652	0.7834	3.4929
R_n_V_c_GRAY_Intrinsic	0.8291	0.9354	0.9743	0.7801	3.5191
GRAY_SA	0.8365	0.9397	**0.9818**	0.7714	3.5296
R_n_GRAY_SA	0.8322	0.9364	0.9735	0.7880	3.5301
GRAY_Intrinsic	0.8344	0.9337	0.9593	0.8316	3.5591
RGB	0.8503	0.9419	0.9718	0.8226	3.5867
R_n_RGB	0.8549	0.9428	0.9684	**0.8409**	3.6072
R_n_GRAY_SA_RGB	**0.8590**	**0.9456**	**0.9753**	**0.8272**	**3.6072**

It is evident from Table 1 that: The best overall performance in terms of accuracy and F1-score is obtained with the combination of R_n_GRAY_SA_RGB

The maximum specificity is obtained by combining GRAY with SA.

The best sensitivity is achieved when R_n + RGB are combined. These results show that illumination-derived representations outperform typical RGB input in segmentation by offering complementary information.

Qualitative Results

Representative segmentation outputs from the ISIC 2017 [35] test set are shown in Figure 3, including: Initial dermoscopic pictures Ground-truth masks Masks predicted from various channel combinations The R_n + GRAY + SA + RGB arrangement offers better border estimation and lesion form preservation, which is in line with quantitative results. The model consistently represents lesion outlines more precisely than other combinations, despite occasional modest edge noise. Figure 3 shows a qualitative comparison of the segmentation outcomes on test photos from ISIC 2017.

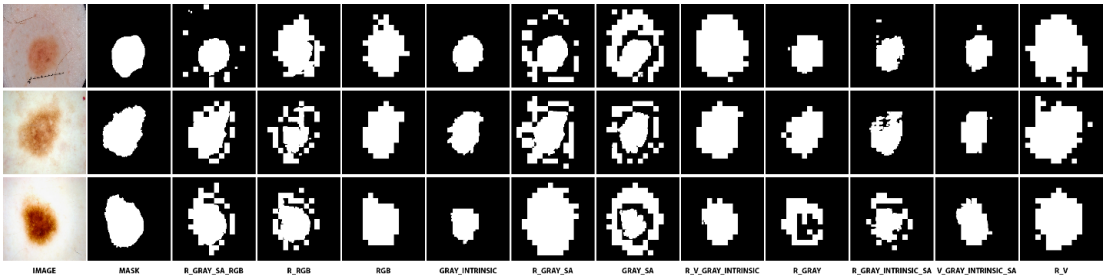


FIGURE 3. Shows the qualitative outcomes of our suggested model using the ISIC 2017 dataset.

DISCUSSION

The outcomes of the experiment show that:

1. For dermoscopic segmentation, RGB is still a reliable baseline representation.

2. Channels formed from illumination, including R_n, GRAY, and SA, have complimentary discriminative characteristics.

3. Without thoroughly analyzing every possible combination, GA-based channel optimization efficiently finds informative channel subsets.

4. The hybrid CNN–Transformer design greatly benefits from multi-channel input optimization.

Overall, the work demonstrates that segmentation performance is enhanced both quantitatively and qualitatively by combining illumination-aware transformations with evolutionary channel selection.

CONCLUSION

This research presented a GA-guided image channel selection for skin lesion segmentation by applying six more changes to RGB dermoscopic pictures. The segmentation outcomes are assessed using a modified TMU-net that can segment inputs with varying channel counts. For skin image segmentation, a genetic algorithm-based image channel selection method is thus presented. The GA-guided technique can choose several characteristics or channels that can improve the overall segmentation outcomes, according to experiments done using the ISIC 2017 dataset. In particular, the tests demonstrate that in addition to RGB, other color transformations including "R_n" "GRAY," and "SA" are crucial for enhancing segmentation outcomes based on various metrics.

It would be very interesting to expand the suggested framework in the future to include additional computer vision tasks including instance segmentation, classification, and detection.

REFERENCES

1. G. P. Guy, S. R. Machlin, D. U. Ekwueme, and K. R. Yabroff, "Prevalence and costs of skin cancer treatment in the U.S., 2002–2006 and 2007–2011," Amer. J. Preventive Med., vol. 48, no. 2, pp. 183–187, Feb. 2015.
2. Yusupov, O. R., Abdiyeva, K. S., Esankulova, B. S., Shamsiyeva, K. G., & Badalova, L. B. (2025, December). Algorithm For Generating Synthetic Mammogram Images Based On The Cyclegan Model. In *2025 IEEE East-West Design & Test Symposium (EWDTS)* (pp. 1-5). IEEE.
3. A. Esteva, B. Kuprel, R. A. Novoa, J. Ko, S. M. Swetter, H. M. Blau, and S. Thrun, "Dermatologist-level classification of skin cancer with deep neural networks," Nature, vol. 542, no. 7639, pp. 115–118, Feb. 2017.
4. R. L. Siegel, K. D. Miller, N. S. Wagle, and A. Jemal, "Cancer statistics, 2023," CA, A Cancer J. Clinicians, vol. 73, no. 1, pp. 17–48, Jan. 2023.
5. R. L. Siegel, K. D. Miller, H. E. Fuchs, and A. Jemal, "Cancer statistics, 2021," CA, Cancer J. Clinicians, vol. 71, no. 1, pp. 7–33, Jan. 2021.
6. S. S. Dake, M. Nguyen, W. Qi Yan, and S. Kazi, ''Human tumor detection using active contour and region growing segmentation,'' in Proc. 4th Int. Conf. Workshops Recent Adv. Innov. Eng. (ICRAIE), vol. 5, Nov. 2019, pp. 1–5.
7. C. M. A. Rahman and H. Nyeem, ''Active contour-based segmentation of Rois in medical images,'' in Proc. Int. Conf. Electr., Comput. Commun. Eng. (ECCE), Feb. 2019, pp. 1–6.
8. A. Kumar, O. S. Ajani, S. Das, and R. Mallipeddi, ''GridShift: A faster mode-seeking algorithm for image segmentation and object tracking,'' in Proc. IEEE/CVF Conf. Comput. Vis. Pattern Recognit. (CVPR), Jun. 2022, pp. 8121–8129.
9. Abduvaitov, A., Shavkatovich Buriboev, A., Sultanov, D., Buriboev, S., Yusupov, O., Jasur, K., & Choi, A. J. (2025). Enhancing Medical Image Segmentation and Classification Using a Fuzzy-Driven Method. *Sensors*, *25*(18), 5931.
10. S. R. Sharma, S. Alshathri, B. Singh, M. Kaur, R. R. Mostafa, and W. El-Shafai, ''Hybrid multilevel thresholding image segmentation approach for brain MRI,'' Diagnostics, vol. 13, no. 5, p. 925, Mar. 2023.
11. U. Ilhan and A. Ilhan, ''Brain tumor segmentation based on a new threshold approach,'' Proc. Comput. Sci., vol. 120, pp. 580–587, Jan. 2017.
12. D. Wu and C. Yuan, ''Threshold image segmentation based on improved sparrow search algorithm,'' Multimedia Tools Appl., vol. 81, no. 23, pp. 33513–33546, Sep. 2022.
13. Fazilov, S. K., Abdiyeva, K. S., Yusupov, O. R., Eshonqulov, E. S., & Esankulova, B. S. (2025, December). Federated Learning Model For Breast Cancer Detection Using Mammogram Images. In *2025 IEEE East-West Design & Test Symposium (EWDTS)* (pp. 1-5). IEEE.
14. Q. Geng and H. Yan, ''Image segmentation under the optimization algorithm of krill swarm and machine learning,'' Comput. Intell. Neurosci., vol. 2022, pp. 1–10, Mar. 2022.
15. T. Zhang, J. Zhang, T. Xue, and M. H. Rashid, ''A brain tumor image segmentation method based on quantum entanglement and wormhole behaved particle swarm optimization,'' Frontiers Med., vol. 9, May 2022, pp. 1–19.
16. Fazilov, S., Yusupov, O., Abdieva, K., Yusupov, R., & Olimjonova, S. (2025, October). Modified ResNet model for breast cancer classification using mammogram images. In *AIP Conference Proceedings* (Vol. 3377, No. 1, p. 060019). AIP Publishing LLC.

17. T. Shen and Y. Wang, ‘‘Medical image segmentation based on improved watershed algorithm,’’ in Proc. IEEE 3rd Adv. Inf. Technol., Electron. Autom. Control Conf. (IAEAC), Oct. 2018, pp. 1695–1698.
18. Fazilov, S.K., Abdieva, K.S., Yusupov, O.R. Patch-based lesion detection using deep learning method on small mammography dataset Artificial Intelligence, Blockchain, Computing and Security - Proceedings of the International Conference on Artificial Intelligence, Blockchain, Computing and Security, ICABCS 2023, 2024, 2, pp. 643–647.
19. J. Long, E. Shelhamer, and T. Darrell, ‘‘Fully convolutional networks for semantic segmentation,’’ in Proc. IEEE Conf. Comput. Vis. Pattern Recognit. (CVPR), Jun. 2015, pp. 3431–3440.
20. O. Ronneberger, P. Fischer, and T. Brox, ‘‘U-Net: Convolutional networks for biomedical image segmentation,’’ 2015, arXiv:1505.04597.
21. S. Cai, Y. Tian, H. Lui, H. Zeng, Y. Wu, and G. Chen, ‘‘Dense-UNet: A novel multiphoton in vivo cellular image segmentation model based on a convolutional neural network,’’ Quant. Imag. Med. Surg., vol. 10, no. 6, pp. 1275–1285, Jun. 2020.
22. X. Tong, J. Wei, B. Sun, S. Su, Z. Zuo, and P. Wu, ‘‘ASCU-net: Attention gate, spatial and channel attention U-Net for skin lesion segmentation,’’ Diagnostics, vol. 11, no. 3, p. 501, Mar. 2021.
23. S. Alryalat, M. Al-Antary, Y. Arafa, B. Azad, C. Boldyreff, T. Ghnaimat, N. Al-Antary, S. Alfegi, M. Elfalah, and M. Abu-Ameerh, ‘‘Deep learning prediction of response to anti-VEGF among diabetic macular edema patients: Treatment response analyzer system (TRAS),’’ Diagnostics, vol. 12, no. 2, p. 312, Jan. 2022.
24. V.M. Opanasenko, S.K. Fazilov, N.M. Mirzaev, S. S. Kakharov, A Model of Recognition Algorithms Based on Threshold Functions and Object Proximity Assessment. Cybernetics and Systems Analysis, 61(1), 148-160. 2025.
25. Nuritdinov, J., Kakharov, S., Tashxodjayev, A., “Application of Minkowski operator in artificial intelligence tasks”, In AIP Conference Proceedings (Vol. 3244, No. 1). AIP Publishing, November, 2024, https://doi.org/10.1063/5.0241599.
26. M. Z. Alom, M. Hasan, C. Yakopcic, T. M. Taha, and V. K. Asari, ‘‘Recurrent residual convolutional neural network based on U-Net (R2UNet) for medical image segmentation,’’ 2018, arXiv:1802.06955.
27. Z. Zhou, M. Siddiquee, N. Tajbakhsh, and J. Liang, ‘‘UNet++: A nested UNet architecture for medical image segmentation,’’ in Proc. Int. Workshop Deep Learn. Med. Image Anal., vol. 11045, 2018, pp. 3–11.
28. J. Nazarov et al., “Genetic algorithm guided image channel selection for skin lesion segmentation,” IEEE Access, vol. 12, pp. 135692–135700, 2024.
29. A. Kumar, G. Hamarneh, and M. S. Drew, ‘‘Illumination-based transformations improve skin lesion segmentation in dermoscopic images,’’ in Proc. IEEE/CVF Conf. Comput. Vis. Pattern Recognit. Workshops (CVPRW), Jun. 2020, pp. 3132–3141.
30. T. Wan, L. Zhao, H. Feng, D. Li, C. Tong, and Z. Qin, ‘‘Robust nuclei segmentation in histopathology using ASPPU-Net and boundary refinement,’’ Neurocomputing, vol. 408, pp. 144–156, Sep. 2020.
31. R. Azad, M. Heidari, Y. Wu, and D. Merhof, ‘‘Contextual attention network: Transformer meets U-Net,’’ in Machine Learning in Medical Imaging, C. Lian, X. Cao, I. Rekik, X. Xu, and Z. Cui, Eds. Cham, Switzerland: Springer, 2022, pp. 377–386.
32. Fazilov, S., Abdieva, K., Yusupov, O., Yusupov, R., & Qodirov, A. (2024, November). A framework utilizing deep learning techniques for the detection and classification of breast cancerous cells in mammographic images. In *AIP Conference Proceedings* (Vol. 3244, No. 1, p. 030082). AIP Publishing LLC.
33. Fazilov, S., Abdieva, K., Yusupov, O., Eshonqulov, E., & Malikov, Z. (2024, November). Re-parameterized Gompertz algorithm for the fuzzy ranks of deep CNN models in the identification of breast cancer using mammography images. In *AIP Conference Proceedings* (Vol. 3244, No. 1, p. 030083). AIP Publishing LLC.
34. Fazilov, S. K., Yusupov, O. R., Abdiyeva, K. S., Abduraxmonov, M. S., & Qodirov, A. A. (2024, November). Comparative analysis of noise reduction filters for the quality enhancement of mammography images. In *2024 IEEE East-West Design & Test Symposium (EWDTS)* (pp. 1-5). IEEE.
35. G. D. Finlayson, M. S. Drew, and C. Lu, ‘‘Intrinsic images by entropy minimization,’’ in Computer Vision—ECCV, T. Pajdla and J. Matas, Eds. Berlin, Germany: Springer, 2004, pp. 582–595
36. A. Madooei, M. S. Drew, M. Sadeghi, and M. S. Atkins, ‘‘Automated pre-processing method for dermoscopic images and its application to pigmented skin lesion segmentation,’’ in Proc. IS&T 20th Color Imag. Conf., 2012, pp. 158–163.
37. M. Hiraoka, M. Firbank, M. Essenpreis, M. Cope, S. R. Arridge, P. V. D. Zee, and D. T. Delpy, ‘‘A Monte Carlo investigation of optical pathlength in inhomogeneous tissue and its application to near-infrared spectroscopy,’’ Phys. Med. Biol., vol. 38, no. 12, pp. 1859–1876, Dec. 1993.

38. N. Tsumura, H. Haneishi, and Y. Miyake, ‘‘Independent component analysis of skin color image,’’ J. Opt. Soc. Amer. A, Opt. Image Sci., vol. 16, no. 9, pp. 2169–2176, 1998.
39. C. Poynton, ‘‘Frequently asked questions about color,’’ Retrieved, no. 449, Jun. 2004.
40. J. Chen, Y. Lu, Q. Yu, X. Luo, E. Adeli, Y. Wang, L. Lu, A. L. Yuille, and Y. Zhou, ‘‘TransUNet: Transformers make strong encoders for medical image segmentation,’’ 2021, arXiv:2102.04306.
41. A. Hatamizadeh, Y. Tang, V. Nath, D. Yang, A. Myronenko, B. Landman, H. R. Roth, and D. Xu, ‘‘UNETR: Transformers for 3D medical image segmentation,’’ in Proc. IEEE/CVF Winter Conf. Appl. Comput. Vis. (WACV), Jan. 2022, pp. 1748–1758.
42. N. C. F. Codella, D. Gutman, M. E. Celebi, B. Helba, M. A. Marchetti, S. W. Dusza, A. Kalloo, K. Liopyris, N. Mishra, H. Kittler, and A. Halpern, ‘‘Skin lesion analysis toward melanoma detection: A challenge at the 2017 international symposium on biomedical imaging (ISBI), hosted by the international skin imaging collaboration (ISIC),’’ in Proc. IEEE 15th Int. Symp. Biomed. Imag. (ISBI), Apr. 2018, pp. 168–172.